Optimal Dispatch and Pricing of Industrial Parks Considering CHP Mode Switching and Demand Response

Yating Zhao, Zhi Wu, *Member*, *IEEE*, *Member*, *CSEE*, Wei Gu, *Senior Member*, *IEEE*, *Senior Member*, *CSEE*, Jingxuan Wang, Fujue Wang, Zhoujun Ma, and Minqiang Hu, *Member*, *IEEE, Member*, *CSEE*

***Abstract*—Industrial parks (IPs) play a crucial role in facilitating economic efficiency and comprehensive energy utilization in the industrial age. At the same time, multi-energy coupling and management of various types of energy in IP have become serious challenges. In this paper, combined heat and power unit (CHP) model considering operation mode switching characteristics is formulated by exploring its internal composition to improve output flexibility of the energy supply side. Then, heat and electricity integrated energy system (HE-IES) optimal dispatch and pricing model are established, taking electricity and heat demand response strategy and steam thermal inertia property into account. Based on the above models, a mixed-integer bilinear programming framework is designed to coordinate the day-ahead operation and pricing strategy of the HE-IES in the IP. The scenario study is carried out on a practical industrial park in Southern China. Numerical results indicate the proposed mechanism can effectively improve IP's energy utilization and economic efficiency.**

***Index Terms*—CHP mode switching, demand response, Industrial park, pricing strategy, steam heating network.**

I. Introduction

NOWADAYS, industrial parks (IPs) thrive and have become a vital pattern to construct modern industry [1]–[3]. IP is an integrated energy system (IES) involving the production, delivery, and utilization of multi-energy sources. Meanwhile, an increasing proportion of renewable energy is integrated into IPs. Its substantial variation and intermittence bring significant challenges to system dispatch. Therefore, the coupling of hybrid energy types, the variable operation state of generation units, changeable demands and irrational energy utilization have become serious issues, which put forward higher requirements for the operation and dispatch of HE-IES.

Combined heat and power (CHP) unit is an essential energy supply equipment in HE-IES that can generate electricity and steam simultaneously [3]. While CHP units usually operate with "heating supply priority", which weakens the flexibility and economy of the HE-IES [4]. Some studies [5]–[8] have focused on the effect of efficiency improvement considering the commitment of flexible devices with CHP units at the system level of the HE-IES. In [5], the impact of using thermal energy storage considering heat transfer to increase the operational flexibility of CHP was analyzed. The commitment of CHP units in the industrial plant was investigated in [6]. Literature [8] discussed the comprehensive effect of CHP units and other energy devices on IES flexibility and REs accommodation. The proposed model of the cogeneration unit schedules thermal and electrical output considering feasible conditions and available data to minimize total operating costs in the plant [9]. However, the internal composition of the CHP unit was simplified or ignored in the above studies. Some other studies [10] analyzed the operation performance of CHP units of the IES from the device level. The internal structure and physical processes of the CHP unit in the dispatch model of IES were first considered in [11]. An economic scheduling model for CHP with logical control was established [10]. Reference [12] regulated key variables in different components to explore the flexibility of CHP plants. By installing bypass systems in turbines or heat storage tanks, the regulation and energy decoupling ability of CHP plants has been significantly improved [13]. However, the mode-switching process was not considered in the above studies. Modeling of physical structures and processes of components in CHP plants has laid a good foundation for the flexibility exploration of CHP plants. In current research on optimized scheduling of HE-IES, the CHP unit operates either in adjustable extraction (AE) mode or in back pressure (BP) mode [14]–[16]. In fact, specific CHP units can switch operation modes without being shut down [10], [17]. Thus, a CHP model considering mode switching processes was applied in this paper to improve the output flexibility of the CHP units for a larger feasible operation range, further enhancing economy and energy utilization efficiency in IP.

The physical heating characteristic was broadly adopted to promote operational flexibility and efficiency of HE-IES [18]–[23]. Considering the temporary mismatch between heat de-

Manuscript received February 21, 2022; revised June 21, 2022; accepted July 7, 2022. Date of online publication December 28, 2023; date of current version July 21, 2024. This work was supported by the National Natural Science Foundation of China (No. 52177077) and by the Science and Technology Project of State Grid Jiangsu Electric Power Co., Ltd., Grant J20210148.

T. Y. Zhao, Z. Wu (corresponding author, email: zwu@seu.edu.cn), W. Gu, J. X. Wang, F. J. Wang and M. Q. Hu are with the School of Electric Engineering, Southeast University, Nanjing 210096, China.

Z. J. Ma is with the College of Energy and Electrical Engineering, Hohai University, Nanjing 210098, China, and also with the State Grid Jiangsu Electric Power Company, Nanjing 210019, China.

DOI: 10.17775/CSEEJPES.2022.01080

mand and supply in thermal systems, the heating network model utilized heat storage property [18]. District heating network (DHN) model in IES optimal dispatch considering flow and temperature details inside the plant was formulated in [19], [20]. A more accurate and practical thermal dynamic model in DHN was explored to describe storage capacity adequately [21]. The economic dispatch model taking building thermal inertia into account was developed in [22], [23]. However, the works mentioned above mainly consider heat hydraulics as heat transfer mediums in pipelines or utilize heat-building storage properties. As a matter of fact, industrial heat demands usually involve high temperatures and high-pressure steam [24]. Some studies have been done on steam pipe network operation [25]–[27], establishing the simulation model to analyze and optimize steam flows in steam heating network (SHN). At the same time, the above models contain nonconvex terms and are complicated, degrading the solvability of the optimization model. Therefore, this paper derives a steam pipe optimization model through some simplifications and approximations. Based on this model, a joint steam and electricity dispatch model is established considering the hydraulic inertia of SHNs. Additionally, energy storage characteristics of steam pipelines can buffer heat output and demand without comprising strict heat balance constraints, contributing to a higher ability to adjust energy supply and demand.

IP is a complex energy system with various energy forms and flexible and adjustable capacity. Demand response (DR) technology can adjust output planning of multi-energy generation systems and demand configuration of consumers in HE-IES [28]. Therefore, a more reasonable thermoelectric ratio will be obtained, increasing theincome of IPO. A DR model is developed to achieve abetter economic dispatch scheme for various electric devices in IP [29]. Time-of-use (TOU) and reward-based DR programs are utilized for DR aggregators to trade DR volumes in electricity markets in IPs [30]. However, as an essential demand type in HE-IES, heat energy property is less considered in the above studies. In [4], factories in the IP are incentivized to change electricity and heat load based on theproposed DR scheme. An integrated demand response (IDR) model considering load-shedding and resource-shifting of hybrid energy is designed to maximize the economic efficiency of multiparty in IPs [31]. Although some research has been done on the implementation of IDR in IES, the interaction between energy generation and the dynamic price of both heat and electricity in IPs still deserves further exploration.

The main contributions of this paper are as follows:

1) A detailed model for switchable CHP unit considering mode switching rule during transition processes will be discussed, and internal physical composition is investigated under each mode in detail.

2) A simplified steam pipe model is developed, and its effectiveness is validated. Based on this model, a steam-and-electricity-integrated dispatch model with thermal steam storage property in IPs is established, aiming to maximize profit of industrial park operator (IPO) and minimize cost of industrial park consumers (IPCs).

3) The pricing mechanism is integrated into the above model, in which the relationship between energy generation and the dynamic price of electricity and heat is studied.

The remainder of this paper is organized as follows. Section II discusses operating mechanism and develops the model of switchable CHP unit. Optimal operation and pricing mechanism considering IDR program in HE-IES is formulated in Section III. Section IV demonstrates feasibility of developed model and method by conducting scenario studies on a practical industrial park. Finally, conclusions are drawn in Section V.

II. Modeling of Switchable CHP

A. Operation Mechanism of CHP Units

According to the difference in exhausted steam pressure, the CHP unit can be classified into BP and AE modes. Flexibility of CHP can be explored by modeling the physical process with internal composition of CHP. Fig. 1 displays simplified but typical structure of a switchable CHP unit, which mainly comprises boiler, steam turbine, as well as auxiliary components. Steam turbine of CHP unit contains a high-pressure cylinder (HPC), an intermediate-pressure cylinder (IPC), and a low-pressure cylinder (LPC) [11].

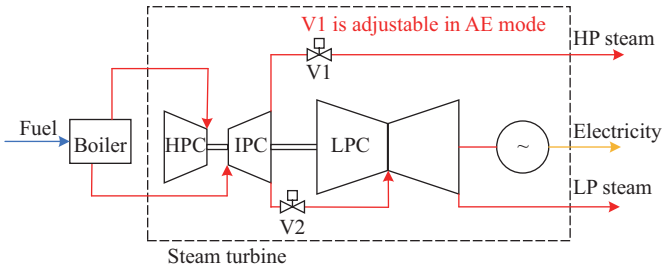

Fig. 1. The simplified structure of the switchable CHP system.

The switching between AE (mode I) and BP (mode II) modes can be realized by controlling and adjusting the valves of different pipelines. The valve after IPC (i.e., V1) is off for BP mode. The boiler consumes coal to generate steam, which works sequentially in the HPC, IPC, and LPC. Exhaust steam from the turbine is all supplied to the SHN. In other words, the back-pressure CHP unit uses low-pressure (LP) steam for heat supply. For AE mode, V1 is on and can be adjusted. Control of the opening degree of V1 can determine the mass flow of steam extracted from the IPC, delivering both LP and medium-pressure (MP) steam for heat supply. Therefore, the thermoelectric ratio in BP mode is fixed, providing little flexibility to various multi-energy demands. In comparison, the thermoelectric ratio of AE mode is more flexible by adjusting the physical structure of the CHP unit.

Thus, it is a foreseeable method to make full use of thecombination of two operation modes. Our paper assumed flexibility as the ability of energy supply units to respond to changing load demands and energy outputs [13].

B. Operation Region of Switchable CHP System

Safe operation region of switchable CHP unit is illustrated in Fig. 2, which shows flexibility of heat and electricity

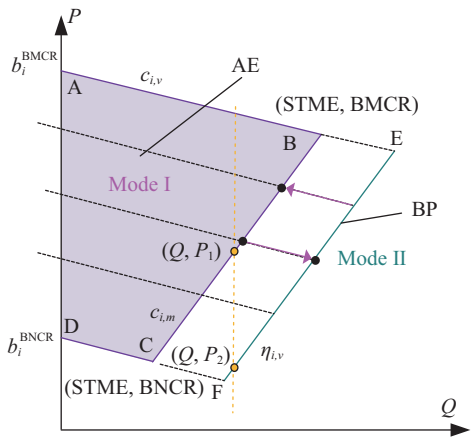

Fig. 2. The operation region of switchable CHP.

production. Heat and electricity output power of model is limited by operating conditions of the boiler and steam turbine, which include boiler maximum continuous rating (BMCR), gas turbine minimum continuous rating (BNCR), and steam turbine maximum extraction (STME).

1) Safe Operation Range of AE Mode

For AE mode, its feasible operating domain is a two-dimensional area surrounded by several operational curves as depicted in line ABCD. Operation constraints are listed in (1)–(4).

$$\varepsilon_{i,t}^{\dagger}\underline{p}_{i,t}^{\dagger} \le p_{i,t}^{\dagger} \le \varepsilon_{i,t}^{\dagger}\overline{p}_{i,t}^{\dagger},\ \forall i,t \tag{1}$$

$$\varepsilon_{i,t}^{\dagger}\underline{h}_{i,t}^{\dagger} \le h_{i,t}^{\dagger} \le \varepsilon_{i,t}^{\dagger}\overline{h}_{i,t}^{\dagger},\ \forall i,t \tag{2}$$

$$p_{i,t}^{\mathrm{I}} \ge \max\{b_i^{\mathrm{BNCR}} - c_{i,v}h_{i,t}^{\mathrm{I}}, b_{i,0} + c_{i,m}h_{i,t}^{\mathrm{I}}\},\ \forall i,t \tag{3}$$

$$p_{i,t}^{\mathrm{I}} \le (b_i^{\mathrm{BMCR}} - c_{i,v}h_{i,t}^{\mathrm{I}}),\ \forall i,t \tag{4}$$

where subscript t is the time of scheduling periods. i is the index of the CHP unit. Ω^{CHP} is the set of indices of CHP units. T is the set of indices of scheduling periods.† can be I or II, indicating operational constraints in mode I or II. $p_{i,t}^{\dagger}$ and $h_{i,t}^{\dagger}$ are the electricity and heat output of CHP unit i at time t under mode †. $\varepsilon_{i,t}^{\dagger}$ is a binary variable denoting the operation state of CHP unit i at time t under mode †, of which value 1 is online state and value 0 is offline state. $\overline{p}_{i,t}^{\dagger}/\overline{h}_{i,t}^{\dagger}$ and $\underline{p}_{i,t}^{\dagger}/\underline{h}_{i,t}^{\dagger}$ are maximum and minimum electricity/heat output values of CHP unit i at time t. $c_{i,v}$ and $c_{i,m}$ are slopes of operation boundary curve AB and BC. b_i^{BMCR}, b_i^{BNCR}, and $b_{i,0}$ are intercepts of operation curves AB, CD, and BC.

2) Safe Operation Range of BP Mode

For BP mode, electricity output change with heat output linearly, operating on line EF. Its operation domain complies with constraints (1)–(2) and (5).

$$p_{i,t}^{\mathrm{II}} = \eta_{i,v}h_{i,t}^{\mathrm{II}} + b_{i,v},\ \forall i,t \tag{5}$$

where $\eta_{i,v}$ is the thermoelectric ratio of the CHP unit. $b_{i,v}$ is the intercept of curve EF.

3) Full Model of the CHP System

In summary, the whole output of the switchable CHP unit is shown in (6). Equation (7) denotes it runs in no more than one mode in each period.

$$\begin{cases} p_{i,t}^{\mathrm{CHP}} = p_{i,t}^{\mathrm{I}} + p_{i,t}^{\mathrm{II}} \\ h_{i,t}^{\mathrm{CHP}} = h_{i,t}^{\mathrm{I}} + h_{i,t}^{\mathrm{II}} \end{cases},\ \forall i,t \tag{6}$$

$$\varepsilon_{i,t}^{\mathrm{I}} + \varepsilon_{i,t}^{\mathrm{II}} \le 1,\ \forall i,t \tag{7}$$

where $p_{i,t}^{\mathrm{CHP}}$ and $h_{i,t}^{\mathrm{CHP}}$ are the output of electricity and heat of CHP unit i at time t.

4) Startup and Shutdown Time Constraints

The minimum startup and shutdown time constraints for AE/BP mode of CHP unit are described as (8).

$$\begin{cases} \sum_{\tau=t-t_i^{\mathrm{X}-}+1}^{t} s_{i,\tau}^{\dagger} \le \varepsilon_{i,t}^{\dagger} \\ \varepsilon_{i,t}^{\dagger} - \varepsilon_{i,t-1}^{\dagger} = s_{i,t}^{\dagger} - e_{i,t}^{\dagger} \end{cases},\ \forall i,t \tag{8}$$

where $s_{i,t}^{\dagger}$ is a binary variable, of which value 1 means the CHP unit i is switched to mode † at period t and 0 otherwise. $e_{i,t}^{\dagger}$ is binary variable, of which value 1 means the CHP unit i is switched from mode † at period t and 0 otherwise. $\underline{t}^{\dagger}$ is minimum online time for CHP unit i in mode †.

5) Switch Times Constraint

Maximum switching times between different modes of CHP units during the whole scheduling period are described as (9).

$$\sum_i \sum_t o_{i,t}^{ae} + o_{i,t}^{bp} \le \overline{\mathrm{N}},\ \forall i,t \tag{9}$$

where $\overline{\mathrm{N}}$ represents the maximum mode switching times of the switchable CHP unit.

III. Combined Electricity and Steam Dispatch and Pricing Model in the Industrial Park

In this section, SHN model considering operation thermal inertia characteristics is formulated first. Then, the IDR program with heat and electricity load adjustment and dynamic pricing is introduced. Based on above model, joint electricity and steam dispatch model aims to optimize economic efficiency of both IPO and IPCs. Thus, the proposed mixed-integer bilinear problem with multi-objective is solved through certain linearization approaches.

A. SHN Constraints

Pipeline modeling and topology constraints modeling are taken into account to establish the SHN model, which is then simplified and solved.

1) Steam Pipeline Modeling

Many existing studies have been done on modeling of steam pipelines [25]–[27]. In general, unsteady steam flow in pipeline can be described by conservation equations of mass, momentum, and energy, state equation, and enthalpy equation. However, these equations are too complex for optimization, so simplifications are necessary [24].

Simplification 1. Diameter of pipes is negligible compared with length of steam pipelines. Furthermore, steam parameters in the section are considered to be uniformly distributed. Thus, steam in a pipeline is always viewed as a single-phase one-dimensional steady flow in steam transportation model [24].

Simplification 2. Steam in SHN, which usually runs in a fixed and narrow range, exhibits characteristics close to ideal

gas. Therefore, we employ the ideal gas formula to construct an approximate SHN model with acceptable error.

Based on Newton's second law of motion, the momentum conservation equation of steam in pipelines can be written as:

$$\frac{\partial(\rho v^2)}{\partial x}+\frac{\partial(\rho v)}{\partial t}+\frac{\partial P}{\partial x}+g\sin\theta+\rho\frac{\lambda v^2}{2d}=0 \tag{10}$$

where ρ is steam density. v is steam flow velocity. P is steam pressure. x is the length along the pipe axis. t is time. θ is the angle between the pipe direction and the horizontal direction. λ is the friction coefficient. d is the internal diameter of the pipe. g is the acceleration of gravity.

Schematic diagram for simplified steam network is depicted in Fig. 3. In (10), first term is inertia term, second term is convection term, and fourth term is gravity term. According to model assumptions and actual situation, the three terms above can be ignored. Specific reasons and detailed formula derivation processes are provided in Appendix A. Hence, simplified expression of momentum conservation equation is as (11).

$$\overline{Q}_{jk,t}^2=\frac{1.2337d_{jk}^5[\mu_1(P_{j,t}^2-P_{k,t}^2)+\mu_2(P_{j,t}-P_{k,t})]}{\lambda_{jk}L_{jk}\sigma_{jk}} \quad \forall j,k,t \tag{11}$$

where λ_{jk} is the friction resistance coefficient of pipe jk. L_{jk} is the length of pipe jk. Considering influence of local resistance loss of the pipe, flow efficiency factor σ_{jk} is introduced. Reference [32] gives the specific value of σ_{jk} under different pipe pressure. d_{jk} is the internal diameter of pipe jk. $P_{j,t}$ and $P_{k,t}$ denote the inlet and outlet pressure of pipe jk at time t. Values of μ_1 and μ_2 can be referred to in Appendix A. $\overline{Q}_{jk,t}=(Q_{j,t}+Q_{k,t})/2$ is the average steam flow in pipe jk at time t. $Q_{j,t}$ and $Q_{k,t}$ are the inlet and outlet steam flow rate of pipe jk at time t.

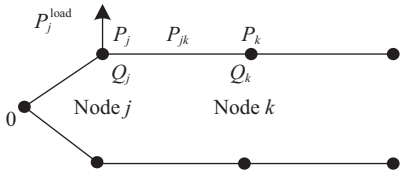

Fig. 3. Schematic diagram for the steam pipe.

Nonlinear terms (i.e., average flow squared $\overline{Q}_{jk,t}^2$ and pressure squared $P_{j,t}^2$) must be linearized to reach global optimality. Then, the piecewise linearization method is applied, and (11) is transformed into (12). Detailed approximation process and related parameters are given in Appendix B.

$$\frac{F(Q_{j,t})+F(Q_{k,t})}{2}=\frac{1.2337d_{jk}^5[\mu_1(F(P_{j,t})-F(P_{k,t}))+\mu_2(P_{j,t}-P_{k,t})]}{\lambda_{jk}L_{jk}e_{jk}} \quad \forall j,k,t \tag{12}$$

2) Topology Constraints

Similar to the circuit principle, each node in the SHN satisfies the KCL constraint, i.e., the sum of steam injected into each node is zero. Subsequently, the node equation of node j can be described as (13).

$$\sum_{k\in\Omega_j^{\text{in}}}Q_{k,t}-\sum_{j\in\Omega_j^{\text{out}}}Q_{j,t}+Q_{j,t}^{\text{load}}=0,\ \forall j,k,t \tag{13}$$

where Ω_j^{in} and Ω_j^{out} represent the set of pipes flowing into and out of node j at time t. $Q_{j,t}^{\text{load}}$ denotes the injected steam load of node j at time t.

3) Energy Storage Capacity

Concerning the pipe pack, a certain amount of steam can be stored in the pipe due to difference between inlet and outlet flow. Thus, pipe inventory $S_{jk,t}$ complies with mass conservation as shown in (14). More specific calculation processes can be referred to [28].

$$\underline{S}_{jk}\le S_{jk,t}=S_{jk,t-1}+Q_{j,t}-Q_{k,t}\le\overline{S}_{jk},\ \forall j,k,t \tag{14}$$

where $\underline{S}_{jk}$ and $\overline{S}_{jk}$ denote the minimum and maximum storage level of pipe jk.

4) Variables Upper and Lower Limits

Each node in SHN has lower and upper pressure, temperature, and load bounds.

$$\begin{aligned}\underline{P}_j\le P_{j,t}\le\overline{P}_j,\ \forall j,t\\ \underline{T}_j\le T_{j,t}\le\overline{T}_j,\ \forall j,t\\ \underline{Q}_j^{\text{load}}\le Q_{j,t}^{\text{load}}\le\overline{Q}_j^{\text{load}},\ \forall j,t\end{aligned} \tag{15}$$

where $T_{j,t}$ is the nodal temperature of node j at time t. $\underline{P}_j$ and $\overline{P}_j$ represent the minimum and maximum values of nodal pressure of node j. $\underline{T}_j$ and $\overline{T}_j$ represent the minimum and maximum values of the nodal temperature of node j. $\underline{Q}_j^{\text{load}}$ and $\overline{Q}_j^{\text{load}}$ represent the minimum and maximum values of nodal load of node j.

5) Heat Balance Constraints

$$\sum_{i\in\Omega^{\text{CHP}}}h_{i,t}^{\text{CHP}}=\sum Q_{0,t} \tag{16}$$

Equation (16) means the sum of thermal output of all centralized heat sources is equal to the sum of inlet steam flow of all steam pipes connected to heat sources at each time, which is described by $\sum Q_{0,t}$.

B. Electrical Power System Constraints

The model we established pays more attention to flexible output scheduling of source-side energy supply equipment (such as CHP units) and energy response of load-side demand. Additionally, IP is a small-scale integrated energy system in which safe operation conditions can be met without considering voltage and capacity problems accurately. Therefore, the electrical power system is treated as a single-node model. Power system constraints are given by (17)–(25). Equation (17) shows the balance constraints for total electric supply and demand. Equation (18) shows ramping up and down rate constraints of CHP units. Equation (19) indicates photovoltaic consumption constraint. Equations (20)–(25) present electrical energy storage (EES) system constraints.

$$\sum_{i\in\Omega^{\text{CHP}}}p_{i,t}^{\text{CHP}}+p_t^{\text{PV}}+p_t^{\text{DIS}}=p_t^{\text{CH}}+p_t^{\text{D}},\ \forall i,t \tag{17}$$

$$-\mathrm{Rd}_i \le p_{i,t}^{\mathrm{CHP}} - p_{i,t-1}^{\mathrm{CHP}} \le \mathrm{Ru}_i,\ \forall i,t \tag{18}$$

$$0 \le p_t^{\mathrm{PV}} \le p_t^{\mathrm{PV,max}},\ \forall t \tag{19}$$

$$0 \le p_t^{\mathrm{CH}} \le p_t^{\mathrm{CH,max}} u_t^{\mathrm{CH}}, \forall t \tag{20}$$

$$0 \le p_t^{\mathrm{DIS}} \le p_t^{\mathrm{DIS,max}} u_t^{\mathrm{DIS}},\ \forall t \tag{21}$$

$$u_t^{\mathrm{CH}} + u_t^{\mathrm{DIS}} \le 1,\ \forall t \tag{22}$$

$$E_{t+1} = E_t + \theta^{\mathrm{CH}} p_t^{\mathrm{CH}} - (1/\theta^{\mathrm{DIS}}) p_t^{\mathrm{DIS}},\ \forall t \tag{23}$$

$$E_t^{\min} \le E_t \le E_t^{\max},\ \forall t \tag{24}$$

$$E_0 = E_{\mathrm{T}} \tag{25}$$

where $p_{i,t}^{\mathrm{CHP}}$ represents electricity produced by CHP unit i at time t. p_t^{PV} is photovoltaic power generation at time t. p_t^{CH} and p_t^{DIS} are charging and discharging power of the EES at time t. p_t^{D} denotes forecast electrical load at time t. u_t^{CH} and u_t^{DIS} are charging and discharging states of the EES at time t. E_t is the electric storage capacity of the EES at time t. Ru_i and Rd_i represent the maximum ramp-up-and-down rates of CHP unit i. $p_t^{\mathrm{CH,max}}$ and $p_t^{\mathrm{DIS,max}}$ are the maximum charging and discharging power of the EES at time t. θ^{CH} and θ^{DIS} are charging and discharging efficiencies of the EES. $E_t^{\min}$ and $E_t^{\max}$ are minimum and maximum capacities of the EES at time t. E_0 and E_{T} are initial and last storage capacities in the EES.

C. Electricity and heat DR Constraints

Price-based IDR program is a mechanism for encouraging consumers to dynamically manage their energy consumptions in response to time-varying prices of electricity and heat power, thereby optimizing energy supply structure and improving interests of multiparty in IP. At the same time, optimal output combination of each energy supply equipment can be solved. Responsive demand is regarded as elastic to energy prices.

$$\begin{aligned} p_t^{\mathrm{D}} &= p_t^{\mathrm{F}} + p_t^{\mathrm{DR}},\ \forall t \\ p_t^{\mathrm{DR}} &= \alpha p_t^{\mathrm{D}},\ p_t^{\mathrm{F}} = (1-\alpha_e) p_t^{\mathrm{D}},\ \forall t \\ h_t^{\mathrm{D}} &= h_t^{\mathrm{F}} + h_t^{\mathrm{DR}},\ \forall t \\ h_t^{\mathrm{DR}} &= \alpha h_t^{\mathrm{D}},\ h_t^{\mathrm{F}} = (1-\alpha_h) h_t^{\mathrm{D}},\ \forall t \end{aligned} \tag{26}$$

$$\tilde{p}_t^{\mathrm{DR}} = \begin{cases} \overline{p}_t^{\mathrm{DR}}, & \tilde{\lambda}_{e,t} < \underline{\lambda}_{e,t} \\ \underline{p}_t^{\mathrm{DR}} - \frac{\tilde{\lambda}_{e,t}-\underline{\lambda}_{e,t}}{\overline{\lambda}_{e,t}-\underline{\lambda}_{e,t}}(\overline{p}_t^{\mathrm{DR}} - \underline{p}_t^{\mathrm{DR}}), & \underline{\lambda}_{e,t} \le \tilde{\lambda}_{e,t} \le \overline{\lambda}_{e,t},\ \forall t \\ \underline{p}_t^{\mathrm{DR}}, & \tilde{\lambda} > \overline{\lambda}_{e,t} \end{cases}$$

$$\tilde{h}_t^{\mathrm{DR}} = \begin{cases} \overline{h}_t^{\mathrm{DR}}, & \tilde{\lambda}_{h,t} < \underline{\lambda}_{h,t} \\ \underline{h}_t^{\mathrm{DR}} - \frac{\tilde{\lambda}_{h,t}-\underline{\lambda}_{h,t}}{\overline{\lambda}_{h,t}-\underline{\lambda}_{h,t}}(\overline{h}_t^{\mathrm{DR}} - \underline{h}_t^{\mathrm{DR}}), & \underline{\lambda}_{h,t} \le \tilde{\lambda}_{h,t} \le \overline{\lambda}_{h,t},\ \forall t \\ \underline{h}_t^{\mathrm{DR}}, & \tilde{\lambda}_{h,t} > \overline{\lambda}_{h,t} \end{cases} \tag{27}$$

$$\begin{aligned} \sum_t \tilde{p}_t^{\mathrm{DR}} &= \sum_t p_t^{\mathrm{DR}},\ \forall t \\ \sum_t \tilde{h}_t^{\mathrm{DR}} &= \sum_t h_t^{\mathrm{DR}},\ \forall t \\ \sum_t \tilde{\lambda}_{e,t}(p_t^{\mathrm{F}} + \tilde{p}_t^{\mathrm{DR}}) &\le \sum_t \lambda_{e,t} p_t^{\mathrm{D}},\ \forall t \end{aligned} \tag{28}$$

$$\sum_t \tilde{\lambda}_{h,t}(h_t^{\mathrm{F}} + \tilde{h}_t^{\mathrm{DR}}) \le \sum_t \lambda_{h,t} h_t^{\mathrm{D}},\ \forall t \tag{29}$$

where $\lambda_{e,t}/\lambda_{h,t}$ and $\tilde{\lambda}_{e,t}/\tilde{\lambda}_{h,t}$ indicate initial and dynamic electricity/heat prices at time t. $\tilde{p}_t^{\mathrm{DR}}/\tilde{h}_t^{\mathrm{DR}}$ is the response result of price-sensitive electricity/heat load at time t, α_e/α_h denotes the predetermined proportion of flexible electricity/heat load. $\underline{\lambda}_{e,t}/\underline{\lambda}_{h,t}$ and $\overline{\lambda}_{e,t}/\overline{\lambda}_{h,t}$ are threshold prices. $\underline{p}_t^{\mathrm{DR}}/\underline{h}_t^{\mathrm{DR}}$ and $\overline{p}_t^{\mathrm{DR}}/\overline{h}_t^{\mathrm{DR}}$ are minimal and maximal values of flexible electricity loads. Equation (26) denotes forecast electricity/heat load. $p_t^{\mathrm{D}}/h_t^{\mathrm{D}}$ consists of a fixed part $p_t^{\mathrm{F}}/h_t^{\mathrm{F}}$ and a flexible part $p_t^{\mathrm{DR}}/h_t^{\mathrm{DR}}$. The relationship between electricity/heat dynamic price and flexible load at each period can be expressed as continuous non-linear functions in (27) [33]. Equation (28) means the whole amount of energy consumption over the day is constant. Electricity/heat expenditure should be reduced after utilizing the DR program, as shown in (III-C).

D. Objective Function

The comprehensive objective function is to maximize the profit of IPO and minimize the energy purchasing cost of IPCs. Profit can be described as the difference between energy sale revenue and the cost of fuel consumption and CHP operation.

$$\max f_1 = C^{\mathrm{Retail}} - C^{\mathrm{CHP}} - C^{\mathrm{ST}} \tag{30}$$

where C^{Retail} represents the energy sale revenue of IPO. C^{CHP} indicates coal consumed by CHP units; C^{ST} is start-up and shut-down cost of CHP units.

$$\begin{aligned} C^{\mathrm{Retail}} &= \sum_t \left[\tilde{p}_{e,t}(p_t^{\mathrm{F}} + \tilde{p}_t^{\mathrm{DR}}) + \tilde{p}_{h,t} \sum_j Q_j^{\mathrm{load}} \right] \\ C^{\mathrm{CHP}} &= \sum_{t\in\mathrm{T}} \sum_i a \left(p_{i,t}^{\mathrm{CHP}} + c_v p_{i,t}^{\mathrm{CHP}} \right)^2 \\ &\quad + b \left(p_{i,t}^{\mathrm{CHP}} + c_v p_{i,t}^{\mathrm{CHP}} \right) + c \\ C^{\mathrm{ST}} &= c_{st} \sum_t \sum_i (s_{i,t}^{\mathrm{I}} + s_{i,t}^{\mathrm{II}}),\ \forall i,t \end{aligned} \tag{31}$$

where a, b and c are cost coefficients of coal consumption of CHP units. c_{st} is the cost of the unit switching operation process.

The energy purchasing cost of IPCs is described as follows.

$$\min f_2 = \sum_{t\in\mathrm{T}} C_t^{\mathrm{Retail}} \tag{32}$$

Different weights are usually set for each target, converting a multi-objective optimization problem into a compound single-objective optimization problem. The weight objective function can be written as (33)[34].

$$F = \min\{-\alpha_1 f_1 + \alpha_2 f_2\} \tag{33}$$

where $\alpha_1 + \alpha_2 = 1$; if preference parameters are set, optimal function F can be achieved.

Finally, the mixed-integer bilinear optimization problem can be formulated as:

$$\begin{aligned} &\min_x(-\alpha_1 f_1 + \alpha_2 f_2) \\ &x := \left\{ p_{i,t}^{\mathrm{CHP}}, h_{i,t}^{\mathrm{CHP}}, \tilde{\lambda}_{e,t}, \tilde{\lambda}_{h,t}, s_{i,t}^{\mathrm{I}}, s_{i,t}^{\mathrm{II}} \right\} \end{aligned} \tag{34}$$

Subject to

(1)–(9), (12)–(III-C).

IV. Case Study

A. Test System and Scenarios

Simulation is performed on the HE-IES of a practical Industrial Park in Wuxi, China, actual data is used. The average power load is 25 MW and the peak power load is 30 MW. A large amount of industrial heat (steam) is needed during processing and production, and it consumes with more than 900,000 t annual heat consumption. The simplified topology of the system is shown in Fig. 4(a). The electric power network consists of 4 MW/32 MWh energy storage power stations and 19 MW PV power stations. The SHN, which has four steam pipelines with a total length of 20.69 km and 15 heat load nodes, is coupled with the EPN at node 1 through committed CHP units. Fig. 4(b) shows the detailed composition of committed CHP units, comprised of 3 steam boilers, two back-pressure CHP units, two switchable CHP units, and steam pipes. Available PV power and total electricity and steam load curves are shown in Fig. 5. Relevant network parameters are provided in Table I, and pipeline information can be obtained from Appendix B.

TABLE I
Equipment Parameters

Parameter	Value	Parameter	Value	Parameter	Value (MW)
b_i^{BNCR}	3	$b_{i,0}$	0.5	$E_t^{\max}$	8
b_i^{BMCR}	15	$\eta_{i,v}$	0.22	$E_t^{\min}$	2
$c_{i,v}$	0.1	θ^{CH}	0.91	$p_t^{\mathrm{CH,max}}$	6
$c_{i,m}$	0.22	θ^{DIS}	0.90	$p_t^{\mathrm{DIS,max}}$	6

All tests are performed on a computer with eight processors running at 3.60 GHz with 16 GB of memory. Programs are coded under MATLAB 2020a environment and programmed with YALMIP by calling GUROBI.

Five scenarios are discussed to verify the effectiveness of

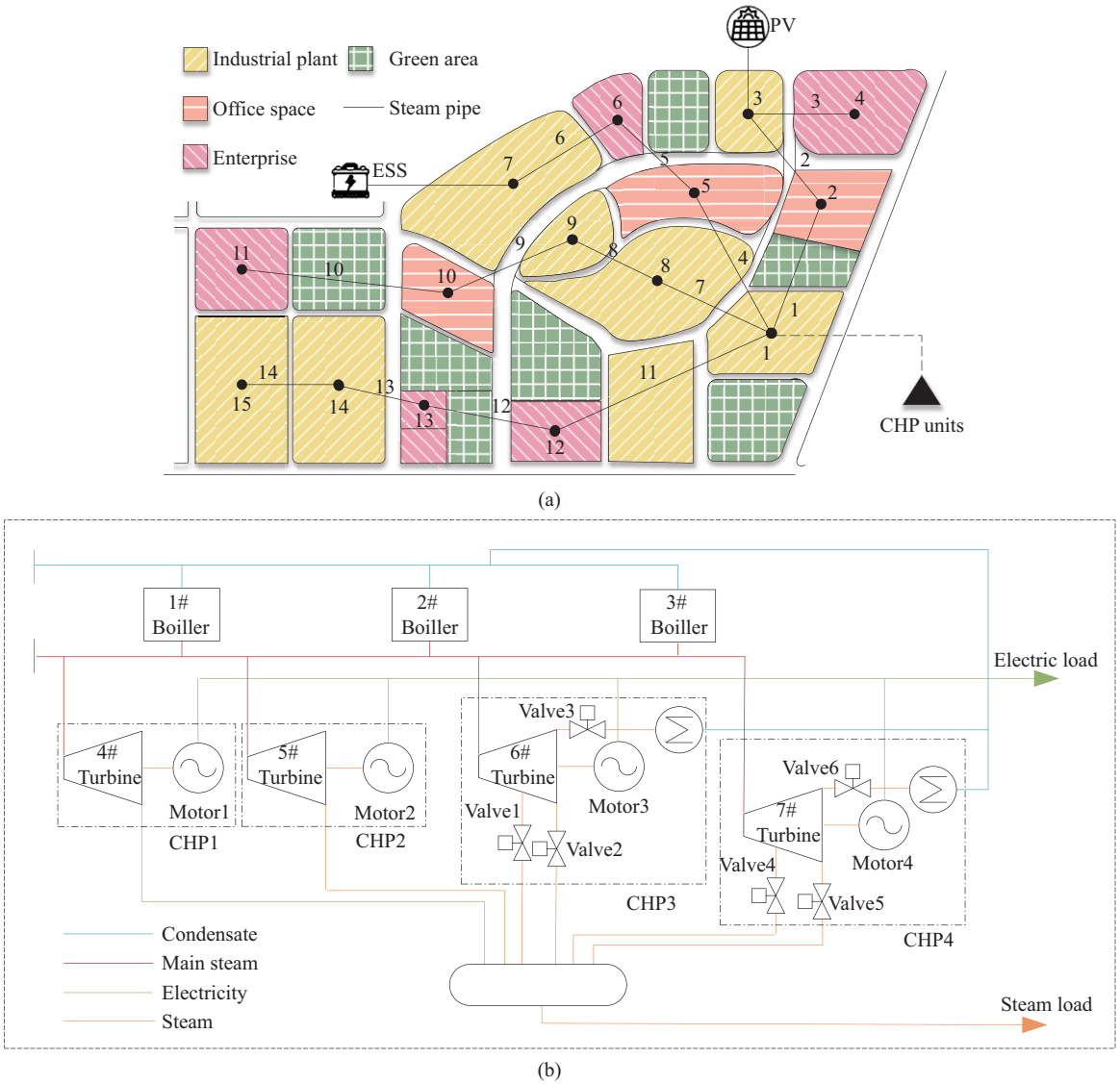

Fig. 4. The topology of practical IP and the detailed commitment of centralized CHP plants. (a) The topology of practical IP. (b) The detailed commitment of centralized CHP plants.

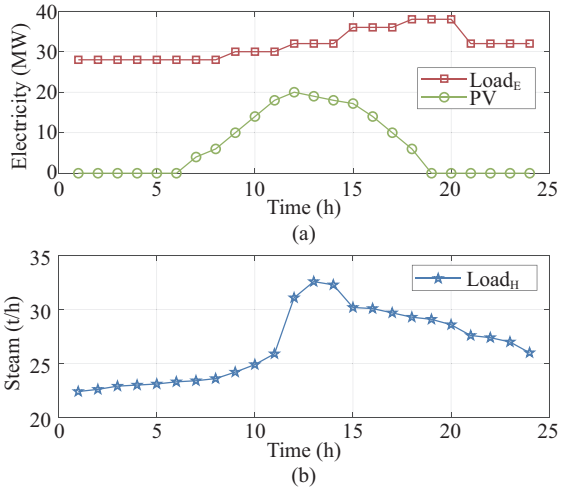

Fig. 5. Profiles of (a) electricity load and PV power forecast output and (b) steam load.

TABLE II
TEST SCENARIOS

Scenario	Mode Switch	DR Mechanism	Characteristic of SHN
1	–	–	–
2	√	–	–
3	√	–	√
4	–	√	√
5	√	√	√

the proposed model as listed in Table II.

In scenarios 1–2, heat dispatch follows heat balance constraints (i.e., the sum of heat output of committed CHP is equal to heat demand at each dispatch period) as shown in (35). While scenarios 3–5 satisfy the operational constraints of SHN stated in (12)–(16).

$$\sum_{i\in\Omega_{\mathrm{CHP}}} h_{i,t}^{\mathrm{CHP}} = h_t^{\mathrm{D}}$$
$$h_t^{\mathrm{D}} = \sum_j Q_{j,t}^{\mathrm{load}} \tag{35}$$

B. Effect of CHP Mode Switch Mechanism

Table III presents the performance comparison of scenarios 1–5. Profit represents the total operating profit of IPO. Payoff denotes the energy purchasing cost of IPCs. Coal indicates the total fuel cost of CHP units. PV represents the total energy utilization of photovoltaic farms over the scheduling horizon. As shown in Table III, the optimal profits of IPO in Scenarios 1 and 2 are \$39,938.47 and \$49,455.12. The operating costs of CHP units in Scenarios 1 and 2 are \$206,645.01 and \$193,982.36. Thus, the optimal profit of IPO is increased by 23.82%, and the operating cost of CHP units declines by 6.13% after considering the switching mechanism of CHP units. Moreover, the PV curtailment in Scenario 2 is saved by 12.63% compared with Scenario 1. The increase of PV accommodation gains from mode switching capability of CHP units. Scheduling results of Scenario 1 and Scenario 2 are shown in Figs. 6 and 7.

Table IV presents the operating mode and switching status of CHP3 and CHP4 units at each dispatch interval. It can be

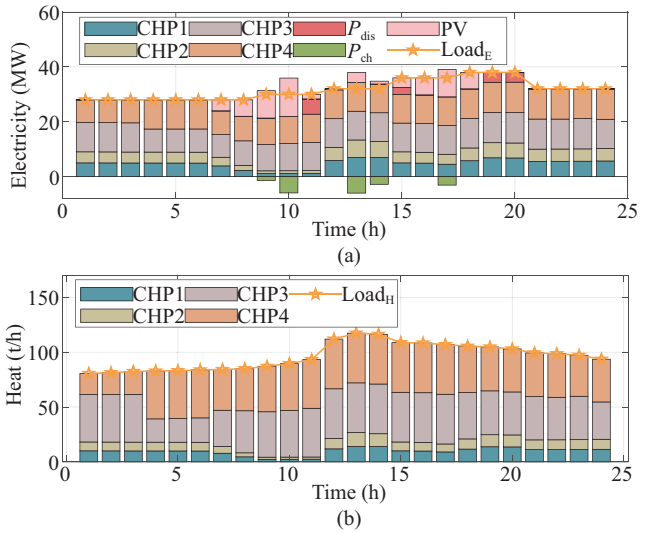

Fig. 6. Scheduling results in Scenario 1. (a) Electricity power output and forecast electricity load. (b) Heat power output and forecast heat load.

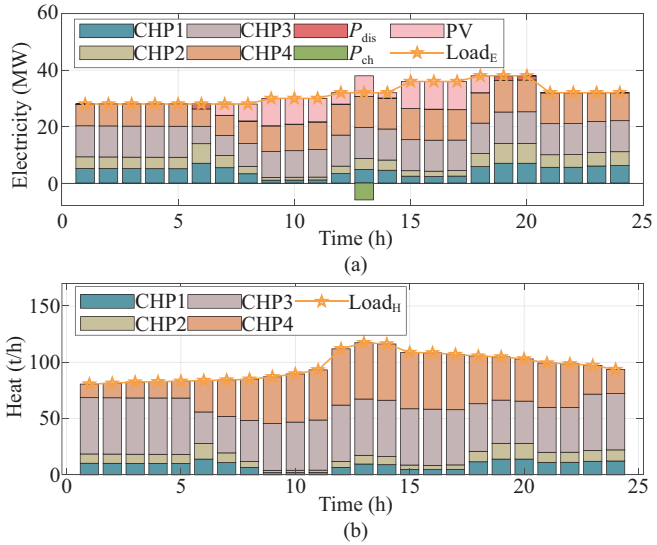

Fig. 7. Scheduling results in Scenario 2. (a) Electricity power output and forecast electricity load. (b) Heat power output and forecast heat load.

TABLE III
RESULTS COMPARISON OF THE FIVE SCENARIOS

Scenario	Profit ($\times 10^3$ \$)	Payoff ($\times 10^3$ \$)	Coal ($\times 10^3$ \$)	PV (%)
1	39.94	246.58	206.64	42.31
2	49.46	246.58	193.98	54.94
3	79.86	226.83	146.16	99.30
4	85.45	240.92	155.48	84.26
5	103.82	240.01	135.40	100.00

seen from Table IV that in a dispatch period, the operation mode of CHP4 unit has been switched twice. At 6:00, CHP4 switches from mode AE to mode BP and runs in mode BP until 17:00. Then it switches to mode AE. Scheduling results can be explained by results in Table IV, which consider the operating characteristics of the switchable CHP unit. When steam demand pertains to a high level with relatively low electricity demand, CHP3 and CHP4 can operate under mode

TABLE IV
OPERATING MODE STATUS OF CHP

Hour	CHP3		CHP4		Hour	CHP3		CHP4		Hour	CHP3		CHP4	
	AE	BP	AE	BP		AE	BP	AE	BP		AE	BP	AE	BP
1	0	1	1	0	9	0	1	0	1	17	0	1	0	1
2	0	1	1	0	10	0	1	0	1	18	1	0	1	0
3	0	1	1	0	11	0	1	0	1	19	1	0	1	0
4	0	1	1	0	12	0	1	0	1	20	1	0	1	0
5	0	1	1	0	13	0	1	0	1	21	1	0	1	0
6	0	1	0	1	14	0	1	0	1	22	1	0	1	0
7	0	1	0	1	15	0	1	0	1	23	0	1	1	0
8	0	1	0	1	16	0	1	0	1	24	0	1	1	0

BP with lower electricity output. Thus, aggregated CHP units decrease electricity output (under the same steam demand level as Scenario 1) to meet both electricity and steam demands, and there is more room for PV power accommodation, leading to lower operating cost of CHP units and higher profit for IPO in Scenario 2. While in Scenario 1, electricity and heat output are limited by their technology boundaries.

Scenarios 4 and 5 in Table III show the effect of the mode switching mechanism on energy scheduling and the interests of all parties after considering the energy storage characteristics of the SHN. The optimal profit of IPO in scenario 5 is \$18,370 more than that in scenario 4, increased by 21.49%. Compared with scenario 4, PV accommodation in scenario 5 increases by 15.74%. While the energy purchasing cost of IPCs and the operating cost of CHP units decrease by \$910 and \$20,080 in scenario 5 (fell by 0.40% and 12.91%), respectively, compared with scenario 4. Thus, considering the mode transition processes the CHP unit contributes to the improvement of energy utilization and economic efficiency.

C. The Storage Characteristic of SHN

In Scenario 2, the total steam output of CHP and total steam demand maintain balance at each hour. At the peak time of PV (10:00–14:00), the CHP unit retains a high-power output due to the fixed steam output, as shown in Fig. 7. Although CHP3 and CHP4 switch to BP mode (which means generating less electricity output when satisfying the same steam demand), there is still a significant PV curtailment. In comparison, the joint dispatch mode utilizing the heat storage characteristic of SHN in Scenario 3 obtains more flexibility. As shown in Figs. 8, before the peak time of PV, aggregated CHP units enhance their total output to meet the increasing flexible electricity demand, and excess steam is stored in the SHN. Then, stored steam is released at the peak time of PV (10:00–14:00), which provides a larger power gap for PV utilization and helps decrease the output of the CHP units, reducing the coal consumption cost of CHP units. Under constraints of SHN operation, the actual steam demand shifts to the period of low steam price, so the purchasing cost of IPCs is reduced. Consequently, the profit of IPO is increased. These results imply that the flexibility enhancement in HE-IES is owing to the energy storage capability in pipelines in SHN.

D. Effect of IDR Mechanism on System Performance

It can be observed in Fig. 9 that after applying the DR program of energy demand and price in Scenario 5, the profit

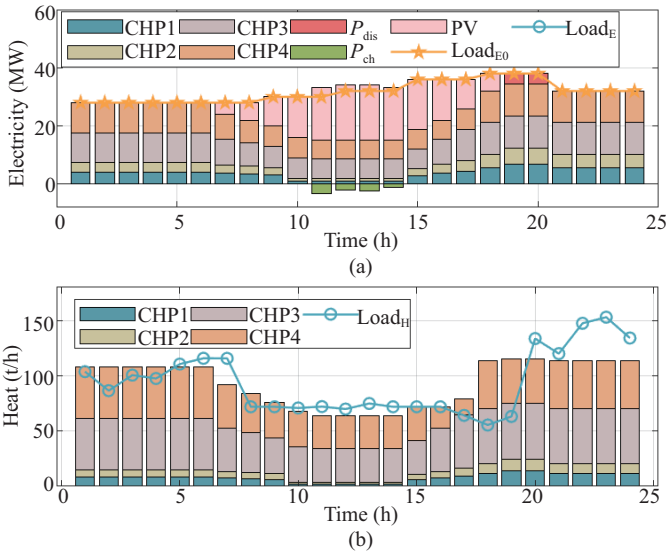

Fig. 8. Scheduling results in Scenario 3. (a) Electricity power output and forecast electricity load. (b) Heat power output and forecast heat load.

of IPO increased by 30.01% compared with that in Scenario 3. Moreover, the fuel cost of CHP units in Scenario 5 declines by 7.34% compared with that in Scenario 3. Note, in Fig. 9(b), electricity prices show a rise in 0:00–11:00 and 17:00–24:00 while a reduction from 11:00 to 17:00, compared with the initial price. Correspondingly, flexible electricity loads mainly move from 17:00–24:00 to 6:00–17:00, as shown in Fig. 9(a). In Fig. 9(d), it is obvious heat price directly relates to steam demand, which indicates heat price falls when demand for heat load is high. The CHP units increase heat output at low-price periods and store excess steam. Heat output is decreased flexibly at high-price periods, and stored steam is released, as shown in Fig. 9(c). Thus, more PV power can be accommodated as more flexible demands shift to the midday hour, and the energy purchase cost of IPCs can be saved effectively. Additionally, when flexible demands increased, corresponding prices declined within the given limit, meeting the goal of optimizing the economic efficiency of both IPO and IPCs.

In Fig. 10(a), bars denote the difference between total steam output and demand, representing the state of charge in SHN. Accordingly, average pressure in SHN weighted by corresponding pipeline mass flow varies with stored energy, as shown by the curve in Fig. 10(b). When the steam difference is negative, indicating total steam output is lower than the steam load, the SHN is discharged, and pressure drops. When the heat difference is positive, the SHN is charged, and pressure is raised, indicating an increase in the internal energy of pipeline steam. Thus, the SHN functions as energy storage to buffer heat output and demand, as well as decouples generation dispatch of CHPs and heat demand, providing more flexibility without compromising strict heat balance constraints.

Moreover, the optimal result of the SHN model used in this paper is compared with the simulation results of a more accurate model. Compared with practical measured data, the biases of the simulation model as control are acceptable in most cases. Thus, it can be used to measure the accuracy

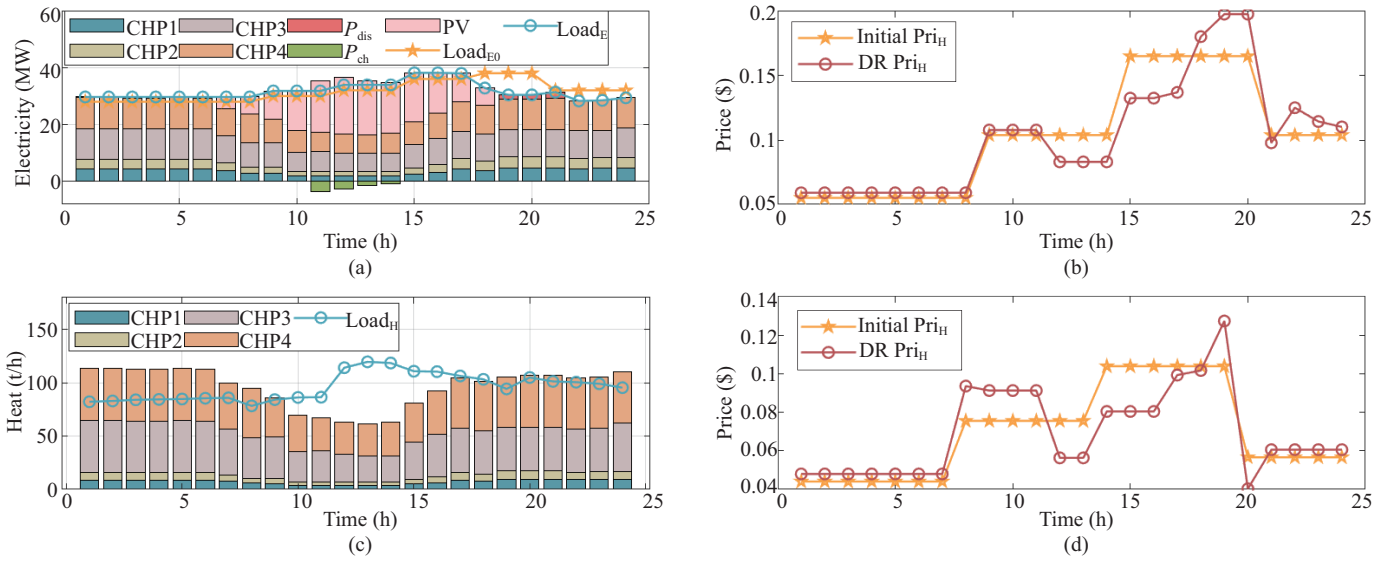

Fig. 9. Scheduling and pricing results in Scenario 5. (a) Electricity output and DR load. (b) Electricity DR price. (c) Steam output and demand. (d) Steam DR price.

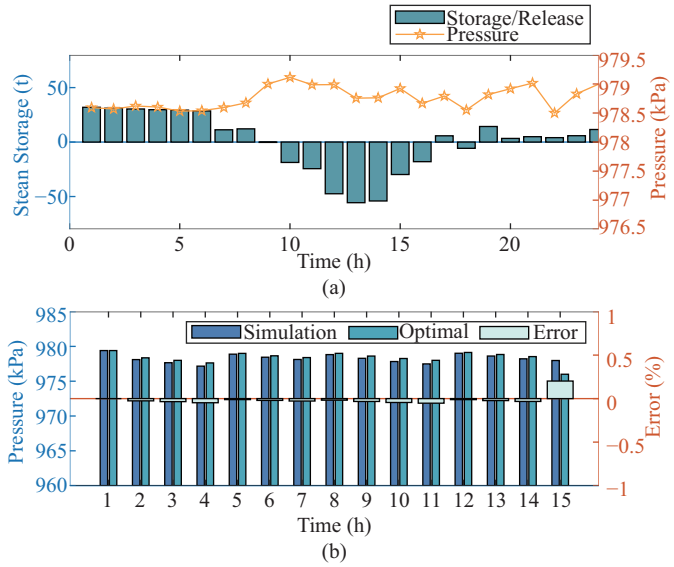

Fig. 10. Operating results in Scenario 5. (a) Steam storage and pressure in SHN. (b) Pressure error between the proposed model in this paper and the accurate simulation model.

and effectiveness of the model proposed in this paper. See Appendix D for details of this model. Fig. 10(b) displays the pressure of all pipelines at certain hours under two models. From Fig. 10(b), the error between the proposed model and the accurate simulation model is within $\pm 0.2\%$, validating the feasibility of the proposed SHN model in this paper.

V. Conclusion and Future Directions

The joint dispatch and pricing model of IES in this paper comprises the CHP mode switching model, the thermal inertia model of SHN, and the IDR model. Through theoretical analysis and case study, the following conclusions can be drawn:

1) Considering the mode transition processes of the CHP unit can significantly improve the flexibility of energy supply.

2) The inertia characteristic of steam pipeline in SHN can buffer heat output and demand during operation period, and schedule of device output becomes more flexible.

3) The IDR program of demand and price contributes to more elastic energy supply and demand relationship. Corresponding change of price can increase economy.

The case study of practical IP indicates the proposed mechanism provides the IES with higher operating flexibility, resulting in higher operation and economic efficiency, more photovoltaic accommodation, and less coal consumption.

Based on the proposed joint dispatch model, several interesting directions are open for future study.

1) How to form a more accurate SHN and solve the highly complicated dispatch model more effectively are still noteworthy topics.

2) It will be a significant task to extend the proposed model and improve calculation efficiency under the condition of uncertain renewable power generation and electric and steam demands in the IES.

Appendix A

Certain terms can be ignored for the following reasons.

1) Given the steady flow state of steam in pipelines, steam parameters have nothing to do with time t and are consistent at any time, so the inertia term can be ignored.

2) From the engineering point of view, the convection term in the formula is meaningful only when the gas flow velocity is very high (close to the speed of sound). While the flow velocity of steam in the steam heating system is generally much smaller than the speed of sound, the convection term can also be ignored.

3) According to actual steam heating system parameters, when elevation difference of steam pipe network is not large, gravity term can also be ignored.

Based on the statements above, the momentum balance equation of steady steam flow can be simplified as:

$$\frac{\partial P}{\partial x}+\rho\frac{\lambda v^2}{2d}=0 \tag{A1}$$

The mass flow of steam has the following relationship with steam density, flow velocity and internal diameter.

$$Q=\rho vA=\frac{\pi\rho v d^2}{4} \tag{A2}$$

Equation (A1) can be transformed into (A3) by replacing v in terms of (A2).

$$\partial P+\rho\frac{\lambda Q^2}{2d\rho A^2}\partial x=0 \tag{A3}$$

In general, steam density ρ is influenced by pressure P and temperature T, which greatly increases the complexity of solving the equation. When steam is saturated, ρ can be regarded as the function of P alone. Thus, ρ can be eliminated by using the relation between ρ and P of saturated steam. Therefore, the fitting relation between ρ and P is used in this paper, and the fitting value is piecewise linearized. In each pressure range, the relative error of the fitting relation is within $\pm 2\%$. The expression is as follows.

$$\rho=\mu_1 P+\mu_2 \tag{A4}$$

where μ_1 and μ_2 can be obtained by looking at Table V [32].

TABLE AI
FITTING COEFFICIENT VALUE OF SATURATED STEAM

Pressure Range (MPa)	μ_1 ($\times 10^{-6}$)	μ_2 ($\times 10^{-6}$)
0.10–0.32	5.2353	0.0816
0.32–0.70	5.0221	0.1517
0.70–1.00	4.9283	0.2173
1.00–2.00	4.9008	0.2465
2.00–2.60	4.9262	0.1992

Based on the above approximation approach, the differential equation (A3) can be reformulated as (11) by replacing A with $A=\pi(d/2)^2$ and integrating.

APPENDIX B

Note constraint (11) contains quadratic terms. Therefore, a piecewise approximation method depicted in Fig. B1 is adopted for linearization to handle the problem. For pipe flow Q_i and node pressure P_i, the upper and lower limits of their values can be obtained according to parameters of practical system, and segment interval can be adjusted according to actual conditions.

Taking Q_i as example, value interval $[Q_i^{\min}, Q_i^{\max}]$ is divided into K-1 segments, and K discrete points satisfy: $Q_i^{\min}=Q_{i,1}\le Q_{i,2}\le\cdots\le Q_{i,K}=Q_i^{\max}$. The function value is $F(Q_{i,k})=Q_{i,k}^2,\ k\in[1,K]$.

The specific approximation process is as follows.

$$F(Q_{i,k})\approx F(Q_{i,1})+\sum_{k\in S}[F(Q_{i,k+1})-F(Q_{i,k})]\delta_k \tag{B1}$$

$$Q_{i,k}\approx Q_{i,1}+\sum_{k\in \mathrm{K}-1}(Q_{i,k+1}-Q_{i,k})\delta_k \tag{B2}$$

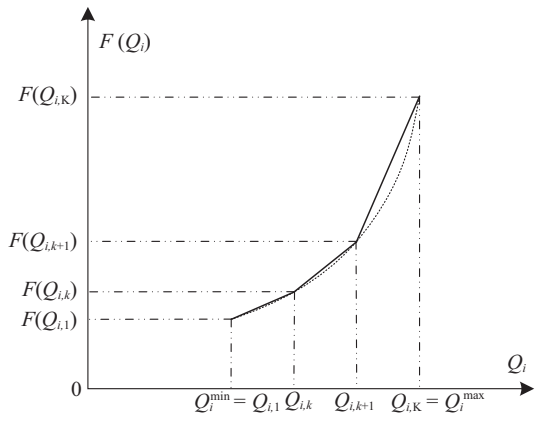

Fig. B1. The piecewise approximation linearization process.

$$\begin{cases}\delta_{k+1}\le\varepsilon_k & \forall k\in K-1\\ \varepsilon_k\le\delta_k\end{cases} \tag{B3}$$

$$0\le\delta_k\le 1\quad\forall k\in K \tag{B4}$$

where K is the number of discrete points. δ_k denotes a continuous variable ranging in [0, 1]. ε_k is a binary variable, used to ensure linearized segments can fill the entire value space continuously from left to right.

APPENDIX C

TABLE CI
SHN PARAMETERS

Pipe ID	From	To	Length (m)	Diameter (m)	Fraction Factor
1	1	2	1510.36	0.8	0.551
2	2	3	1165.64	0.8	0.395
3	3	4	1990.89	0.8	0.531
4	1	5	1489.97	0.8	0.75
5	5	6	1429.17	0.8	0.566
6	6	7	1486.86	0.8	0.75
7	1	8	1388.03	0.8	0.742
8	8	9	1365.4	0.8	0.887
9	9	10	1510.36	0.8	0.551
10	10	11	1165.64	0.8	0.395
11	1	12	1510.36	0.8	0.551
12	12	13	1665.64	0.8	0.395
13	13	14	1790.89	0.8	0.531
14	14	15	1165.64	0.8	0.395

APPENDIX D

Reference [35] demonstrated the method to set up the synthetic model of steam pipeline network based on the hydraulic-thermal model of single pipe, and proposed an algorithm based on Newton-Raphson method to simulate the static flow rate distribution of steam network. The modeling method can be general for most steam pipeline networks.

$$q=C_{\mathrm{P}}(P_1^2-P_2^2) \tag{B5}$$

$$C_{\mathrm{P}j}=\frac{D_j^5\rho_m}{1.25\times 10^8\lambda q P_1(1+\eta)L} \tag{B6}$$

$$q=C_T(T_1-T_2) \tag{B7}$$

$$C_T=\frac{278c_{\mathrm{p}}q^2}{(1+\beta)q_{\mathrm{l}}L} \tag{B8}$$

$$\boldsymbol{q} = \boldsymbol{C}_{\mathrm{P}}^{*}\boldsymbol{A}^{\mathrm{T}}\boldsymbol{P} = \boldsymbol{C}_{\boldsymbol{T}}^{*}\boldsymbol{A}^{\mathrm{T}}\boldsymbol{T} \tag{B9}$$

$$\boldsymbol{A}\boldsymbol{C}_{\mathrm{P}}^{*}\boldsymbol{A}^{\mathrm{T}}\boldsymbol{P} + \boldsymbol{Q} = 0 \tag{B10}$$

$$\boldsymbol{A}\boldsymbol{C}_{T}^{*}\boldsymbol{A}^{\mathrm{T}}\boldsymbol{T} + \boldsymbol{Q} = 0 \tag{B11}$$

where q is the mass flow rate. P_1 and P_2 are input and output steam pressure. D is the inner diameter of the pipe. ρ_m is the weighted mean density of steam. λ is the coefficient of the frictional resistance. L is the length of the pipe. η is the equivalent length coefficient. β is the equivalent length coefficient induced by the appendix of pipes, valves, and supports. According to the different ways of pipes being laid, the value can be selected as 0.15–0.25. c_{p} is the specific heat capacity at constant pressure. q_{l} is the amount of heat loss along unit pipe length. Matrix $\boldsymbol{A}$ represents relationship between the i-th node and the j-th pipe. $\boldsymbol{P} = (P_1^2, P_2^2, \cdots, P_m^2)^{\mathrm{T}}$, P_i, $(i = 1, \cdots, m)$ is the absolute pressure of the i-th node. $\boldsymbol{T} = (T_1^2, T_2^2, \cdots, T_m^2)^{\mathrm{T}}$, $T_i (i = 1, \cdots, m)$ is the i-th node temperature. $\boldsymbol{Q} = (Q_1^2, Q_2^2, \cdots, Q_m^2)^{\mathrm{T}}$, Q_i, $(i = 1, \cdots, m)$ is the flow rate of the i-th node. For steam sources the sign is minus, and for the consumer the sign is positive, otherwise, the value is 0. $\boldsymbol{q} = (q_1, q_2, \cdots, q_{\mathrm{p}})^{\mathrm{T}}$, q_j, $(j = 1, \cdots, p)$ is the flow rate of the j-th pipe. $\boldsymbol{C}_p^{*} = \mathrm{diag}(C_{P1}, C_{P2}, \cdots, C_{Pp})^{\mathrm{T}}$, C_{Pj}, $(j = 1, \cdots, p)$ is the parameter of the j-th pipe determined by (B6); $\boldsymbol{C}_T^{*} = \mathrm{diag}(C_{\mathrm{T}1}, C_{\mathrm{T}2}, \cdots, C_{\mathrm{T}p})^{\mathrm{T}}$, $C_{\mathrm{T}j}$, $(j = 1, \cdots, p)$ is the parameter of the j-th pipe determined by (B8). (B5)–(B8) describe the hydraulic-thermal model of single pipe. (B9)–(B11) describe the synthetic model for steam pipe network.

REFERENCES

[1] A. Hasanbeigi, G. Harrell, B. Schreck, and P. Monga, "Moving beyond equipment and to systems optimization: Techno-economic analysis of energy efficiency potentials in industrial steam systems in China," *Journal of Cleaner Production*, vol. 120, pp. 53–63, May 2016.

[2] P. Xu, Q. S. Bu, Y. Z. Li, J. Geng, J. F. Zhang, and Q. Ying, "Study and simulation of combined cooling heating and power system in an industrial park," in *2020 IEEE 3rd Student Conference on Electrical Machines and Systems*, Jinan, China, 2020, pp. 496–501.

[3] D. Qiu, F. Chen, D. Liu, M. Cao and S. Y. Liu, "Modeling Method of Multi-Energy Systems Based on LSTM Algorithm," *CSEE Journal of Power and Energy Systems*, vol. 10, no. 4, pp. 1701–1709, Jul. 2024.

[4] W. Xiong, Y. Cai, Y. Q. Liu, Y. W. Chen, Q. L. Guo, H. B. Sun, and T. Lei, "Case studies of demand response in multi-energy industrial parks," in *2017 IEEE Conference on Energy Internet and Energy System Integration*, Beijing, China, 2017, pp. 1–5.

[5] X. Y. Chen, C. Q. Kang, M. O'Malley, Q. Xia, J. H. Bai, C. Liu, R. F. Sun, W. Z. Wang, and H. Li, "Increasing the flexibility of combined heat and power for wind power integration in China: modeling and implications," *IEEE Transactions on Power Systems*, vol. 30, no. 4, pp. 1848–1857, Jul. 2015.

[6] Y. H. Dai, L. Chen, Y. Min, P. Mancarella, Q. Chen, J. H. Hao, K. Hu, and F. Xu, "A general model for thermal energy storage in combined heat and power dispatch considering heat transfer constraints," *IEEE Transactions on Sustainable Energy*, vol. 9, no. 4, pp. 1518–1528, Oct. 2018.

[7] C. H. Lin, W. C. Wu, B. Wang, M. Shahidehpour, and B. M. Zhang, "Joint commitment of generation units and heat exchange stations for combined heat and power systems," *IEEE Transactions on Sustainable Energy*, vol. 11, no. 3, pp. 1118–1127, Jul. 2020.

[8] X. Y. Chen, M. B. McElroy, and C. Q. Kang, "Integrated energy systems for higher wind penetration in China: formulation, implementation, and impacts," *IEEE Transactions on Power Systems*, vol. 33, no. 2, pp. 1309–1319, Mar. 2018.

[9] M. I. Santos and W. Uturbey, "A practical model for energy dispatch in cogeneration plants," *Energy*, vol. 151, pp. 144–159, May 2018.

[10] H. Q. Yu, L. O. Nord, C. Yu, J. X. Zhou, and F. Q. Si, "An improved combined heat and power economic dispatch model for natural gas combined cycle power plants," *Applied Thermal Engineering*, vol. 181, pp. 115939, Nov. 2020.

[11] T. Jiang, Y. Min, G. P. Zhou, L. Chen, Q. Chen and F. Xu, "Dispatch model for integrated heat and power systems considering internal composition of CHP plants," *CSEE Journal of Power and Energy Systems*, vol. 7, no. 2, pp. 396–407, Mar. 2021.

[12] S. H. Huang, F. Z. Sun, D. R. Sheng, H. T. Liu, S. Tu, J. M. Yang, and S. C. Li, *The Principles of Turbines*. Beijing: China Electric Power Press, 2008.

[13] J. W. Wang, S. You, Y. Zong, C. Træholt, Z. Y. Dong, and Y. Zhou, "Flexibility of combined heat and power plants: a review of technologies and operation strategies," *Applied Energy*, vol. 252, pp. 113445, Oct. 2019.

[14] M. L. Zhang, Q. W. Wu, J. Y. Wen, Z. W. Lin, F. Fang, and Q. Chen, "Optimal operation of integrated electricity and heat system: A review of modeling and solution methods," *Renewable and Sustainable Energy Reviews*, vol. 135, pp. 110098, Jan. 2021.

[15] J. F. Rist, M. F. Dias, M. Palman, D. Zelazo, and B. Cukurel, "Economic dispatch of a single micro-gas turbine under CHP operation," *Applied Energy*, vol. 200, pp. 1–18, Aug. 2017.

[16] P. D. Ge, Q. R. Hu, Q. W. Wu, X. B. Dou, Z. J. Wu, and Y. Y. Ding, "Increasing operational flexibility of integrated energy systems by introducing power to hydrogen," *IET Renewable Power Generation*, vol. 14, no. 3, pp. 372–380, Feb. 2020.

[17] S. Ding, W. Gu, S. Lu, X. Chen and R. Yu, "Improving Operational Flexibility of Integrated Energy Systems Through Operating Conditions Optimization of CHP Units," *CSEE Journal of Power and Energy Systems*, vol. 9, no. 5, pp. 1854–1865, Sep. 2023.

[18] Z. G. Li, W. C. Wu, M. Shahidehpour, J. H. Wang, and B. M. Zhang, "Combined heat and power dispatch considering pipeline energy storage of district heating network," *IEEE Transactions on Sustainable Energy*, vol. 7, no. 1, pp. 12–22, Jan. 2016.

[19] Z. G. Li, W. C. Wu, J. H. Wang, B. M. Zhang, and T. Y. Zheng, "Transmission-constrained unit commitment considering combined electricity and district heating networks," *IEEE Transactions on Sustainable Energy*, vol. 7, no. 2, pp. 480–492, Apr. 2016.

[20] X. S. Jiang, Z. X. Jing, Y. Z. Li, Q. H. Wu, and W. H. Tang, "Modelling and operation optimization of an integrated energy based direct district water-heating system," *Energy*, vol. 64, pp. 375–388, Jan. 2014.

[21] I. Gabrielaitiene, "Numerical simulation of a district heating system with emphases on transient temperature behaviour," in *Proc. 8th International Conference Environment Engineering*, 2011, pp. 747–754.

[22] Z. G. Pan, Q. L. Guo, and H. B. Sun, "Feasible region method based integrated heat and electricity dispatch considering building thermal inertia," *Applied Energy*, vol. 192, pp. 395–407, Apr. 2017.

[23] S. Lu, W. Gu, K. Meng, S. Yao, B. Liu, and Z. Y. Dong, "Thermal inertial aggregation model for integrated energy systems," *IEEE Transactions on Power Systems*, vol. 35, no. 3, pp. 2374–2387, May 2020.

[24] B. B. Chen, W. C. Wu, C. H. Lin, Q. L. Guo, and H. B. Sun, "Improving flexibility for microgrids by coordinated optimization of electricity and steam networks," *IEEE Transactions on Sustainable Energy*, vol. 12, no. 1, pp. 314–324, Jan. 2021.

[25] Q. T. Liu, Z. G. Zhang, J. H. Pan, and J. Q. Guo, "A coupled thermo-hydraulic model for steam flow in pipe networks," *Journal of Hydrodynamics*, vol. 21, no. 6, pp. 861–866, Dec. 2009.

[26] H. Wang, H. Y. Wang, T. Zhu, and W. L. Deng, "A novel model for steam transportation considering drainage loss in pipeline networks," *Applied Energy*, vol. 188, pp. 178–189, Feb. 2017.

[27] A. García-Gutiérrez, A. F. Hernández, J. I. Martínez, M. Ceceñas, R. Ovando, and I. Canchola, "Hydraulic model and steam flow numerical simulation of the Cerro Prieto Geothermal Field, Mexico, pipeline network," *Applied Thermal Engineering*, vol. 75, pp. 1229–1243, Jan. 2015.

[28] J. X. Wang, H. W. Zhong, Z. M. Ma, Q. Xia, and C. Q. Kang, "Review and prospect of integrated demand response in the multi-energy system," *Applied Energy*, vol. 202, pp. 772–782, Sep. 2017.

[29] W. W. Xu, D. Zhou, X. M. Huang, B. L. Lou, and D. Liu, "Optimal allocation of power supply systems in industrial parks considering multi-energy complementarity and demand response," *Applied Energy*, vol. 275, pp. 115407, Oct. 2020.

[30] M. Z. Oskouei, S. Zeinal-Kheiri, B. Mohammadi-Ivatloo, M. Abapour, and H. Mehrjerdi, "Optimal scheduling of demand response aggregators in industrial parks based on load disaggregation algorithm," *IEEE Systems Journal*, vol. 16, no. 1, pp. 945–953, Mar 2022.

[31] Y. H. Zhao, K. Peng, B. Y. Xu, H. M. Li, Y. Q. Liu, and X. H. Zhang, "Bilevel optimal dispatch strategy for a multi-energy system of industrial parks by considering integrated demand response," *Energies*, vol. 11, no. 8, pp. 1942, Jul. 2018.
[32] X. Liu, "Discussion on the construction of brewery energy management system," *Technology & Orientation*, no. 29, pp. 174, 2012.
[33] W. Wei, J. H. Wang, and L. Wu, "Distribution optimal power flow with real-time price elasticity," *IEEE Transactions on Power Systems*, vol. 33, no. 1, pp. 1097–1098, Jan. 2018.
[34] P. Pujihatma, S. P. Hadi, N. Sarjiya, and T. A. Rohmat, "Combined heat and power multi-objective optimization with an associated petroleum and wet gas utilization constraint," *Journal of Natural Gas Science and Engineering*, vol. 54, pp. 25–36, Jun. 2018.
[35] X. X. Luo, S. B. Liu, M. H. Xu, and H. Ying, "Modeling and simulation of steam pipeline network with multiple supply sources in iron & steel plants," in *Proc. 2016 Chinese Control and Decision Conference (CCDC)*, 2016, pp. 4667–4671.

Yating Zhao received the B.Eng. degree in Electrical Engineering from Nanjing Normal University, Nanjing, China, in 2020. She is currently pursuing the Master degree at the School of Electrical Engineering, Southeast University. Her research interests include the optimized operation of integrated energy system.

Zhi Wu received the M.Sc. degree in Electrical Engineering from the School of Electrical Engineering, Southeast University, Nanjing, China, in 2012, and the Ph.D. degree from the University of Birmingham, Birmingham, U.K., in 2016. He is currently working as an Associate Professor with the School of Electrical Engineering, Southeast University. His research interests include renewable energy, planning, and optimization techniques.

Wei Gu received the B.Eng. and Ph.D. degrees in Electrical Engineering from Southeast University, China, in 2001 and 2006, respectively. From 2009 to 2010, he was a Visiting Scholar with the Department of Electrical Engineering, Arizona State University, Tempe, AZ, USA. He is currently a Professor with the School of Electrical Engineering, Southeast University. His research interests include distributed generations and microgrids, and active distribution networks.

Jingxuan Wang received the B.Eng. degree in Electrical Engineering from Hohai University, Nanjing, China, in 2020. She is currently pursuing the Master degree at the School of Electrical Engineering, Southeast University. Her research interests include integrated energy system optimization and operation research.

Fujue Wang received the B.Eng. degree in Electrical Engineering from Hohai University, Nanjing, China, in 2020. She is currently pursuing the Master degree at the School of Electrical Engineering, Southeast University. Her research interests include optimization and planning of integrated energy system.

Zhoujun Ma received the B.S. and M.S. degrees in Electrical Engineering from Southeast University and Shanghai Jiao Tong University, respectively, in 2009 and 2013, and the Ph.D. degree from Hohai University. He currently works with the State Grid Jiangsu Electric Power Company Co., Ltd., Nanjing Electrical Power Supply Company, Nanjing, China. His research interests include power distribution dispatching, operation and control of power systems, etc.

Minqiang Hu received the Ph.D. degree in Electrical Engineering from the Huazhong University of Science and Technology, Wuhan, China, in 1990. He is currently a Full Professor with the School of Electrical Engineering, Southeast University, Nanjing, China. His research interests include electric machine modeling and simulation, renewable energy generation, distributed generation, and microgrids.